Chapter 10
Amorphous Nanophotonics in Nature

Stephen Luke and Peter Vukusic

Abstract Visual appearance generates stimuli associated with many biological functions, including interspecies and intra species communication. A range of biological structural colour mechanisms has been identified. These mechanisms include highly periodic microstructures associated with bright and saturated colours, and amorphous structures which produce broadband colours and generally diffuse reflectances. In this chapter several highly functional amorphous structures found in biological systems are detailed, and their optical characteristics are described.

10.1 Introduction

Colour production in nature can be broadly separated into two distinct categories, based on two levels of animal morphology [1]. The majority of bright appearances found in nature are derived through chemical pigmentation. These are achieved through selective absorption (or scattering) of particular wavelengths of light. An alternative strategy, one which often results in ultra-bright appearances, is the use of sub-micrometer structures. The interaction of light with these intricate microstructures, constructed from material which itself shows little or no intrinsic optical absorption, can produce vivid colours and often stunning visual effects.

Although this chapter will focus primarily on amorphous structures and broadband appearances, this section will introduce the reader to the field of natural photonics as a whole and will include detail of periodic structures. Presentation of details of all structural colour identified to date would be an enormous task and require considerable space. As such a very brief overview of many of the structural colour mechanisms will be given, using examples to highlight the optical effects associated with the structural types. The majority of colour mechanisms that have been identified employ a periodic structure, in either 1, 2 or all 3 dimensions, and result in bright, narrow-band reflectance. Whilst not strictly the remit of this chapter,

S. Luke (✉) · P. Vukusic
School of Physics, University of Exeter, Exeter, UK
e-mail: S.M.Luke@ex.ac.uk

P. Vukusic
e-mail: P.Vukusic@exeter.ac.uk

C. Rockstuhl, T. Scharf (eds.), *Amorphous Nanophotonics*,
Nano-Optics and Nanophotonics, DOI 10.1007/978-3-642-32475-8_10,
© Springer-Verlag Berlin Heidelberg 2013

an introduction to natural photonics would not be complete without describing the microstructure and optical mechanisms which are responsible for the majority of biological structural colour.

The saturated colours and often brilliant visual effects found in nature have inspired significant scientific study. The earliest record of such study is the work of Robert Hooke, reported in his 1665 publication 'Micrographia' [2]. Hooke correctly concluded that the bright colouration of duck and peacock feathers is a structural effect that arises as the result of the interaction of light with alternating layers of two different materials. Newton also undertook studies of avian colour appearance mechanisms and reached a similar conclusion to that of Hooke, this was described in his work 'Opticks' [3], published in 1704. Significant progress in the field was achieved by Lord Rayleigh who used Maxwell's equations of electromagnetism to develop a theory of reflection from stratified surfaces [4]. A subsequent review of the field, published in 1919, concluded that many bright colours found in birds, beetles and beetles were 'structural colours', resulting from thin film interference, rather than pigmentary colours [5].

Since these early works the invention of the electron microscope has revealed a broad range of structural colour mechanisms associated with many intricate structural designs. Whether the purpose is high reflectivity for intra-specific signalling, cryptic colouration or one of several other possible purposes, such optical systems have evolved to perform a function and have been under continuous evolution, in response to selection pressures for, in some cases, hundreds of millions of years. It is therefore unsurprising to find a diverse array of structural colouration mechanisms in the natural world which are seemingly optimised to perform specific biological functions.

Reviewing the literature concerning natural photonic structure will identify a broad range of optical effects in a broad range of animals and insects. From this literature it is apparent that a large proportion of natural photonics arise from either optical interference associated with multilayer structures or with diffraction associated with surface or bulk periodic structures [1]. Multilayer systems, or 1D photonic crystals comprising alternating layers of high and low refractive index materials, are prolific in nature. While some systems exist in which the multilayering exists in broad flat layers, it is more often incorporated within a more specialist design that is best suited to a specific function, physiology or environment [1]. The *Morpho* genus of butterflies is an often quoted example of a specialised 1D photonic structure. The brilliant blue wings (see Fig. 10.1(a)), quoted as being visible from a quarter of a mile away, arise from the interference of light reflected from the discrete multilayer system contained on *Morpho* wing scales (Fig. 10.1(b)). Absorbing pigments and imperfect periodicity amongst the discrete stacks of layers enhances the saturation of the blue colour and the spread the reflection into a wider angle range [6].

Periodicity in 2D is also a geometry that leads to colour production in nature. An interesting example of structural colour effected by a 2D periodic structure is that exhibited by the marine polychaete worm *Aphrodita* (sea mouse). The sea mouse has a body which is covered in short hair-like structures known as setae which display exceptional iridescence (see Fig. 10.1(c)). The core of each setae comprises a bundle of thin wall chitin tubes held together in a 2D hexagonal packed array. Coherent

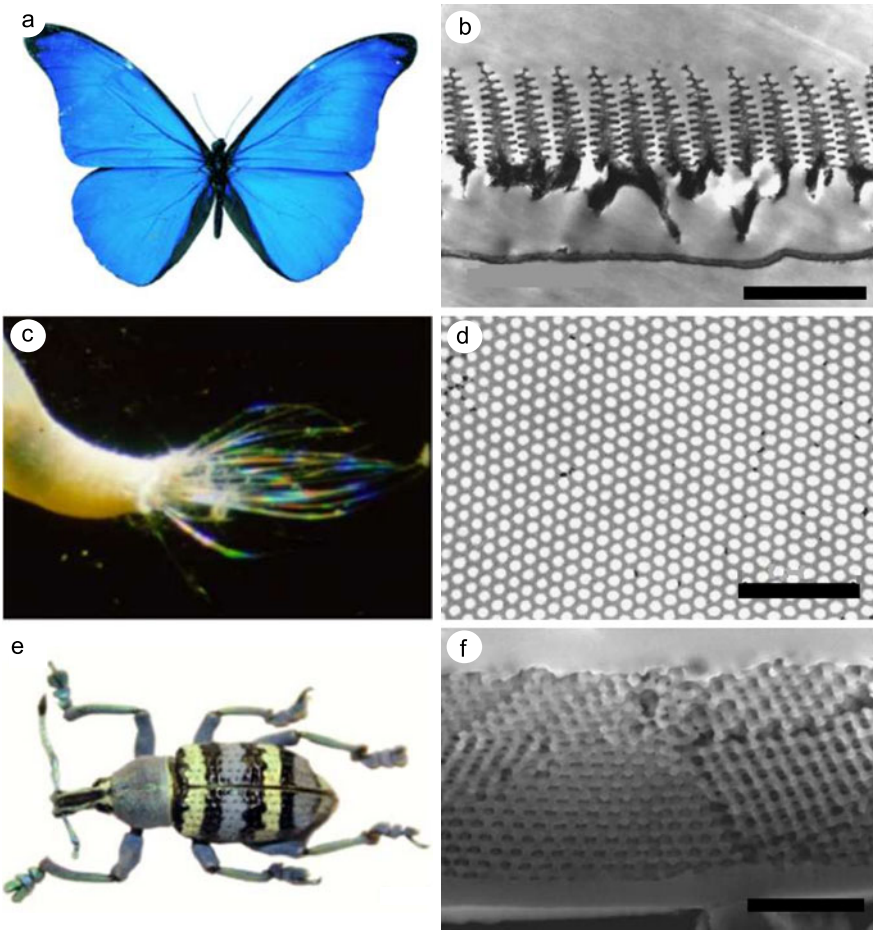

Fig. 10.1 (**a**) Optical image showing the blue iridescent colour of a typical *Morpho* species. (**b**) TEM image of a transverse section through a typical *Morpho* wing scale. Multilayer interference from the 1D periodicity results in the bright blue reflection from the wings. (**c**) Optical image of the 'sea mouse' *Aphrodita*, note the iridescent hair like structures, called setae. (**d**) This iridescence is effected by diffraction from a 2D photonic structure within in setae. (**e**) The weevil *Eupholus magnificus* displays bright blue and green stripes, both colours are structural in origin. (**f**) The green colour results from Bragg scattering of light from a highly ordered 3D photonic crystal within the scales covering the weevils body. *Scale bars*: All 2 μm. (**d**) Reprinted with permission, ©2010, American Physical Society. (**e**) and (**f**) Reprinted with permission, ©2011, Optical Society of America

scattering from this periodic structure results in the coloured reflection. In *Aphrodita* the diameter of the cylindrical tubes varies from 100 nm up to 360 nm, resulting in the large range of reflected colours [1, 7].

Remarkable 3D periodicity has been identified in certain insect species, including both Lepidoptera and weevils. The weevil *Eupholus magnificus* (Fig. 10.1(e)) is

a remarkable example of structural colour as its colour appearance is associated with both fully ordered (Fig. 10.1(f)) and quasi-ordered 3D photonic crystals [8]. Coherent scattering of light from planes of material within the structure creates the yellow–green reflection. The 3D crystal is usually in the form of a poly-crystal, smaller domains of the lattice structure in various orientations formed together to form a solid. For any given illumination, the colour reflected from each domain will depend on its orientation, the macroscopically observed colour is simply a spatial average of the reflection from each domain. Reorienting the crystal changes the reflected colour from each domain but not the system as a whole. Put simply, the domaining of the crystal acts as an iridescence reducing mechanism, believed to help with predator avoidance through camouflage [1, 8].

Broadband scattering systems in nature have been identified and studied but there is not a wealth of literature devoted to the subject. Mason [9] dedicated a portion of his early work on insects to white species. Without the aid of the electron microscope he was unable to inspect the detailed nature of the sub-micron structures but his work has proven to be accurate nonetheless. His work inspected many species of white butterfly with colour appearances ranging from chalky white to highly lustrous, near-metallic whites. He concluded that the differences between the observed effects were due to the differences in microstructure. The chalky matt white of pierid butterflies was caused by uniform scattering in all directions from a disordered arrangement of reflecting surfaces, the uniform nature of the scatter results in a lack of 'high lights' (gloss) [9]. Electron microscopy has since revealed this to be the case. Lustrous whiteness, such as that exhibited by species of the moth genus *Euproctis*, is created by a combination of optical scattering from fine scale structures contained within its relatively transparent scales, and stacking of the scales in layers. The difference between matt white and pearly white, Mason concluded, was dependent on the amount of fine scattering structure. Scales that exhibit minimal scattering structure and scales that overlap in a layered manner often exhibit minimal diffuse scatter and therefore display lustrous, near-metallic whiteness [9].

In this chapter recent discoveries of broadband scattering structures found in nature will be discussed. As for the narrow band examples detailed above the focus will be on insects. Broadband scattering microstructure found in both butterflies and beetles will be discussed, including details of the key structural parameters and the mechanisms by which they function.

10.2 Amorphous Nanostructures in Insects

10.2.1 Lepidopteran Colouration

Some of the brightest colours seen in nature are those displayed by butterflies and moths (order Lepidoptera). Such colouration has inspired a significant amount of scientific interest leading to lepidopteran colour appearance strategies becoming widely studied e.g. [6, 10, 11]. The extensive study of lepidopteran systems has

led to them being amongst the best understood and has led to the identification of a number of diverse structural types.

The name of the order Lepidoptera is derived from the Ancient Greek words for 'scale' and 'wing'. Almost without exception, all members of the order exhibit scales on their wings. It is the scale covering which is largely responsible for wing colouration, either through pigmentation or through microstructure on the surface of, or contained within, the wing scales [10, 11]. Each scale is a flattened projection of cuticle from an epidermal cell within the surface of the wing. Although a large range of scale structures have been identified, most scales conform to a basic pattern, even the most specialised scales share features with basic unspecialised scales. The scales feature a stalk (*petiole*), which fits into a socket on the wing surface, and a main body of the scale (*blade*). The *blade* has two surfaces, the upper and lower *laminae*. The lower *lamina*, which usually faces the wing surface and is not exposed, is usually relatively flat and featureless. The upper *lamina* usually features prominent ridges running from root to tip [10]. These ridges are often seen to be connected by a perpendicular series of cross-ribs, creating *windows* to the empty scale interior. Pillar-like *trabeculae* appear throughout the scale, with the apparent role of separating the upper and lower *laminae* [10].

Pieris Rapae, the Small Cabbage White Butterfly

The small cabbage white butterfly (*Pieris rapae*) is a member of the Pieridae family and is common across much of the world (see Fig. 10.2(a)). Its chalky white colour is structural in origin, resulting from a disordered structure within its wing scales (see Fig. 10.2(b)). *P. rapae* wing scales conform to the basic scale structure previously described, with longitudinal ridges and perpendicular cross-ribs. The specialised part of the scale structure, seen in many pierid species, comprises a dense array of ellipsoidal beads of pterin, contained within the empty void between the upper and lower scale *lamina* (see Fig. 10.2(c)). The array appears to 'hang' from both the ridges and cross-ribs [12, 13]. A gender difference has been noted with males pierids seen to exhibit a much denser bead-array within their scales [14].

Wing colour of the pierid family has been the subject of numerous studies and significant literature exists. Identification of the scale microstructure was not possible prior to the invention of the electron microscope. Studies, therefore, focused on the macroscopically observable properties of the wing. This work revealed the marked gender difference, identified as significantly reduced UV reflectance for males [15, 16]. The strong UV absorption identified is associated with the pterin class of pigments. Pterins are a class of pigments with differing absorption properties. Erythopterin absorbs wavelengths up to approximately 500 nm resulting in the bright yellow colour of many pierid species [17]. Leucopterin absorbs exclusively in the UV and is the likely pigment present in the scales of *P. rapae*.

Early scanning electron microscope (SEM) studies allowed microscopic analysis of the wing scales and revealed the extent of the presence of the ellipsoidal beads suspended from the scale ridges and cross-ribs [18]. Further research later

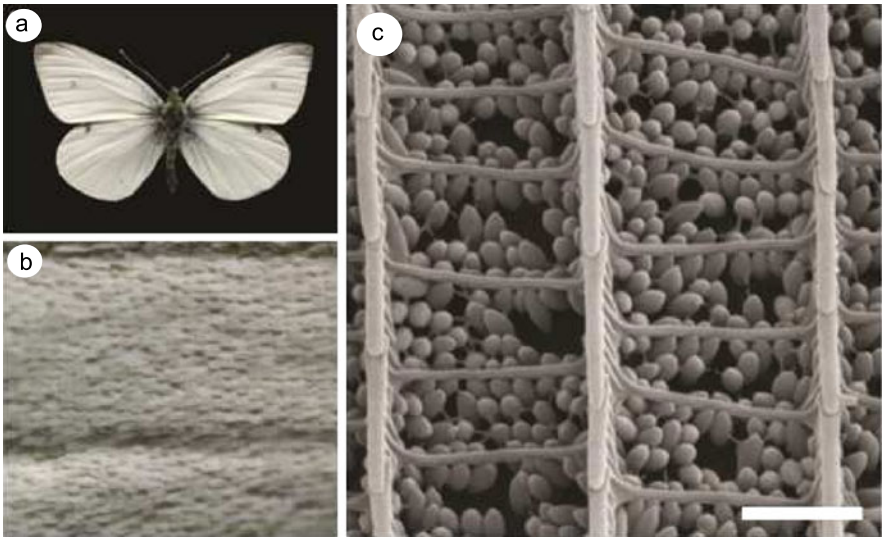

Fig. 10.2 (**a**) Optical image showing the chalky white wings of the small cabbage white *P. rapae*. (**b**) As with the majority of lepidoptera, the wing colouration is effected by a covering of scales. (**c**) *P. rapae* wing scales possess ridges and orthogonal cross-ribs, common to most butterfly species scales. The dense array of ellipsoidal beads is a common feature amongst pierid species. The beads effect both strong UV absorption and enhance visible wavelength light scatter. *Scale bar*: (**c**) 1 μm

concluded that the UV absorbing pigment was is isolated within these dense bead-arrays [19–21].

More recent work by Stavenga et al. has suggested that these beads also play an important role in enhancing broadband light scatter from the wing scales [22]. Morehouse et al. presented evidence for this when they detected a correlation between pterin bead-array density and absolute reflectance of the wings of the pired butterfly *Pontia protodice* [19]. To establish a similar trend for the species *P. rapae* it was necessary to alter the bead-array density of the wing scales of that species. Using a method outlined by Rutowski et al. [21] the pterin beads were dissolved using an immersion technique involving isopropyl alcohol and dilute ammonium hydroxide (NH_4OH). SEM imaging of the wing scales post immersion confirmed the reduction in the bead-array density (see Fig. 10.3).

Initially beads suspended in the scale windows are removed (Fig. 10.3(b)); it is likely that these beads are removed first due to the fragile supporting links which hold them within the windows being dissolved. For longer immersion times (Fig. 10.3 (c) and (d)) the beads appear to dissolve, thereby reducing in volume and eventually number until no beads remain. Bead-array density was calculated for all wing samples after immersion in the NH_4OH solutions. Bead-array density was found to be negatively correlated with immersion time in NH_4OH.

Removal of the bead-array had two principle effects on wing reflectance (Fig. 10.4 (a)). At short wavelengths (400–450 nm) reflectance increased from ca. 8 % for untreated wings to ca. 40 % for wings from which all the beads had been

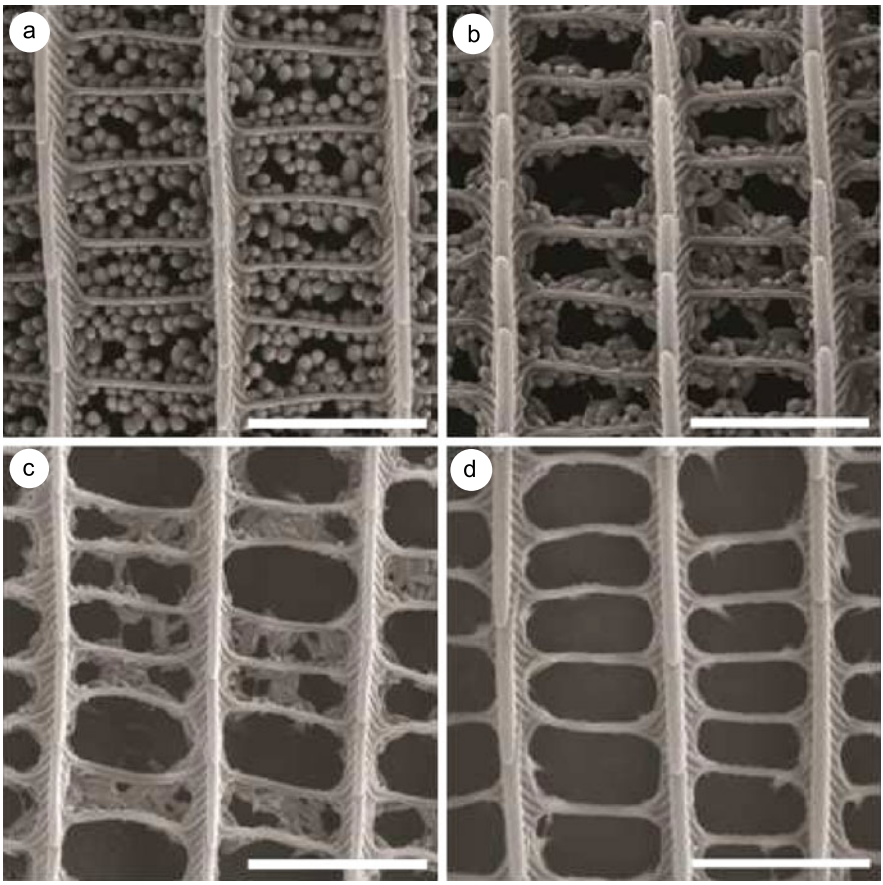

Fig. 10.3 Immersion of *P. rapae* wings in dilute ammonium hydroxide preferentially dissolves the beads over the wing superstructure. Longer immersion times result in greater bead removal. SEM images depicting the extent of the pterin bead array in male *P. rapae wings*: (**a**) Untreated wing; (**b**) after immersion for a short period of time (15–30 seconds); (**c**) after immersion for an intermediate period (60–90 seconds); (**d**) complete bead removal after immersion for approximately 120–150 seconds. *Scale bars*: 2 μm

removed. This is entirely expected due to the removal of the absorption of the pterin pigment associated with the beads. Conversely, reflectance at longer wavelengths was reduced from ca. 65 % for untreated wings to ca. 50 % for treated wings. This is symptomatic of the decrease in optical scatter due to the removal of the pterin bead scattering centres.

At short wavelengths where UV absorption by the pterin pigment is significant, there is a strong negative correlation between total wing reflectance and bead-array density. At a wavelength of ca. 430 nm there appears to be a critical point where the reduction in optical scatter associated with pterin bead removal is balanced by the reduction in optical absorption by the pterin. At approximately this wavelength,

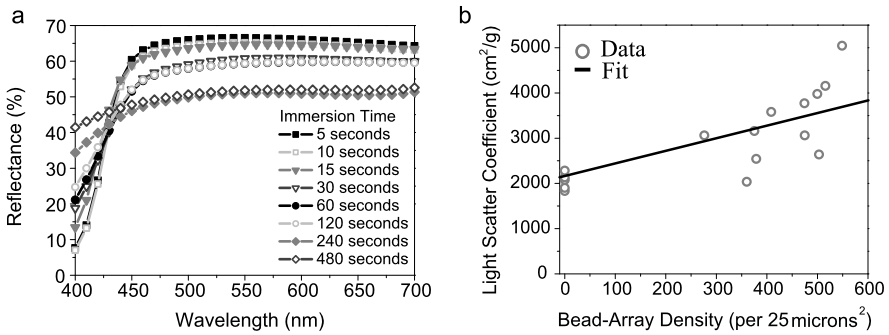

Fig. 10.4 Optical effects of removing the beads from the wing scales of male *P. rapae* butterflies. (**a**) The dual role of the beads is apparent from the reflectance spectra, as the beads are removed UV reflectance significantly increases and visible wavelength reflectance decreases. (**b**) Reflectance spectra were recalculated using Kubelka–Munk theory into an optical scatter coefficient. This quantitatively reveals the extent of non-bead optical scatter

the NH_4OH solution has very little effect on the wing reflectance, despite the major modification of the wing scale structures. At longer wavelengths ($\lambda > 430$ nm), where optical scattering rather than absorption dominates, there is a positive correlation between bead-array density and wing reflectance. This data is consistent with the previous work on *P. rapae* conducted by Morehouse [19] and Stavenga [22], it strongly implies that for *P. rapae*, the wing scale pterin bead-array density is a significant factor in explaining wing reflectance and thus its appearance.

Calculation, using Kubelka–Munk theory [23], of the light scatter coefficient (S) of the wing samples enables their optical properties to be understood more clearly. This technique is regularly used in the paper manufacturing industry where the optical properties of the product are critical. Presented here is a novel application of the theory to a natural scattering system. Figure 10.4(b) shows the relationship between the light scatter coefficient and pterin bead-array density for male *P. rapae* wing scales. Light scatter is observed to increase with increasing bead-array density; this again confirms that the beads are a major contributor to wing reflectance through enhanced optical scatter. This analysis, however, also shows quantitatively that non-bead intra-scale structures contribute to the optical scatter observed [24]. The remaining light scatter results from the bi-grating-like superstrate, or the planar substrate of the wing scale, or a combination of both.

Finite element modelling further indicates the optical scattering role of the scale superstructure. Models consisting of 2D cross-sections through the wing structure were constructed and the simulated scattered power from the system calculated. In the absence of better data, a refractive index of 1.56, similar to that of generic cuticle was used [6]. The pterin absorption profile was also incorporated. The primary focus on the modelling was the presence of the planar scale substrate, an approximately 100 nm thick layer of chitin forming the lower surface of the wing scales. The effect of the presence of the scale substrate is clearly demonstrated in the simulations. Scattered power density in the dorsal hemisphere is significantly increased

when the scale substrate is included in the model. A mean enhancement of approximately 2.54 is observed when the scale substrate is included compared to when it was omitted (over a wavelength range of 300–800 nm). The enhancement factor appears to follow the reflectance spectrum of the substrate indicating that the planar substrate acts as a mirror, reflecting light scattered by the beads and enhancing the scale reflectance. The key result of this modelling is the indication that while the pterin beads enhance optical scatter from the scales, they are not solely responsible for it, in line with the optical data presented by previous research and within this section. The remaining scale structure, specifically the scale substrate, is also a vital component in the scattering system.

Significant research has been conducted on the mating habits of pierid butterflies. Obara [25] and Rutowski [26] suggest that UV absorption by the wings is crucial in distinguishing between males and females. This is particularly the case for *P. r. crucivora* where there is a distinct sexual dimorphism. This dimorphism is not so distinct for British *P. rapae* species, the wing scales of both male and female of which are adorned with beads and subsequently exhibit low UV reflectance [14]. Only at longer, visible wavelengths does the magnitude of the reflectance significantly differ between males and females. Obara and Majerus conducted experiments on British *P. r. rapae* and observed that the lack of distinct sexual dimorphism occasionally led to males approaching other males mistakenly in courtship [27].

Rutowski et al. and Kemp et al. suggest that the UV reflectance generated by wing scales in the butterfly *Colias eurytheme* contains information about the quality of the lamellae-based nanostructure that generates the signal [21, 28], giving an honest indication of the condition of the male butterfly. The contrast in reflectance of short wavelengths ($\lambda < 430$ nm) to that of the longer wavelength region from male *P. rapae* wings is directly correlated to the wing scale pterin bead array-density. This may give a similar indication of the fitness of the individual; this hypothesis would need to be confirmed by behavioural studies.

Morpho Cypris

The brilliant blue colour of the wings of *Morpho* butterfly species is one of the most famous examples of so-called structural colour. In the introduction to this chapter we saw that the scale ridges exhibit discrete multilayering in a ‘Christmas tree’ like microstructure. Multilayer interference of light reflected from the periodic structure results in the vivid blue colouration. A theoretical model has been proposed which explains the extraordinary reflective properties of *Morpho* by introducing the cooperation of the regularity and irregularity of the structure [29].

Among the species of the *Morpho* genus, a few, e.g. *M. cypris* and *M. rhetenor helena*, have a white stripe pattern on their brilliantly coloured blue wings. As whiteness is generally associated with disordered structures and it is found here amongst the vivid blue from a highly ordered structure it begs the question, what structural difference is responsible for the optical difference between the blue and white regions of the wing?

Spatial analysis of both the dorsal (inner surface on closed wings) and the ventral (outer surface) indicate that the white stripe pattern is almost identical on both sides of the wing. Removal of the scales reveals that the pattern is repeated on the wing membrane. SEM analysis reveals that the dorsal scales show little structural variation irrespective of blue or white colouration, all dorsal scales exhibit the tree-like structure with little or no variation in ridge number, size or spacing. The ventral scales exhibit the unspecialised lepidopteran scale structure and again little variation is seen between brown and white scales [30].

Optical measurements of the blue and white dorsal scales reveal in both cases a strong reflectance peak at a wavelength of 470 nm. In spite of this spectral spike, the wing stripe still appears white. The crucial difference between the blue and white scales is revealed in the longer visible wavelength reflectance. Strong absorption in the blue scales results in *ca.* 5 % reflectance for wavelengths longer than 550 nm [30]. For white scales this minimum is *ca.* 30 %. The blue light is still strongly reflected from the white scales (as they have the tree-like structure) but the special reflection properties of the *Morpho* wing negate the effect. The blue light is reflected into a very narrow angular range, due to the anisotropy in the ridge lamella structure. The higher reflectance of blue wavelengths is only applicable in a limited viewing angle, in the rest of the viewing hemisphere diffusely reflected light of all wavelengths is visible, resulting in the white colouration. The dorsal scales also contribute to the reflectance, removal of these scales sees a 10 % drop in reflectance for all visible wavelengths [30].

10.2.2 Disordered Nanostructure in Coleoptera

Coleoptera form the largest and one of the most visually diverse animal orders on earth. Their colour appearances range from extremely matt black through highly saturated visible colours to broadband specularly reflecting surfaces [31, 32], many also have detailed colour patterning [33]. A broad range of diverse structural colour systems has been identified in many different beetles; these include two dimensional surface diffraction gratings such as those found in a number of beetles in the *Serica* genus [34, 35] and three dimensional photonic crystals in the scales of many weevils [36, 37]. However, by far the most common structural colour system in beetles is based on multilayers [33]. Different macroscopic appearances, including iridescent colours and broadband reflection, have been attributed to variations in multilayer design [38–40].

In contrast to the structures described in these highly periodic systems, which create saturated colours and sometimes metallic appearances, the production of whiteness requires an absorption-free microstructure that scatters all optical wavelengths equally. Intense optical scatter from a structure containing many disordered reflecting surfaces is require; it is this disorder that is responsible for the uniformity with which all wavelengths are scattered.

Cyphochilus is a scarab beetle reported to display brilliant whiteness from a surface layer of scales with a thickness of only 5 μm [41]. This remarkable optical performance arises from the interaction of light with a random filamentary microstructure contained within the scales. The *Cyphochilus* system exhibits considerably higher scattering efficiency than a typical synthetic counterpart, delivering comparable optical performance for a significantly smaller layer thickness [41].

The remarkable optical properties of *Cyphochilus* suggest optimisation of the scale design for optimal light scatter. The filament system previously identified can be considered as a collection of discrete scattering centres. In such a system, the phenomenon known as optical crowding reduces scattering efficiency if the scatterers are spaced too closely together [42, 43], the brilliant whiteness of *Cyphochilus* indicates that the scale design is optimised to limit optical crowding.

In this section the optimisation of the light scattering nanostructure within *Cyphochilus* scales and those of two further white beetle species, *Lepidiota stigma* and *Calothyrza margaritifera*, is detailed. *Cyphochilus* (Fig. 10.5(a)) is a member of the Scarabaeidae family, often known as scarab beetles. *Lepidiota stigma* (Fig. 10.5(c)) is a chafer beetle also of the Scarabaeidae family. *Calothyrza margaritifera* (Fig. 10.5(e)) is a member of the Cerambycidae family, also known as longhorn beetles or longicorns. All three species are native to south-east Asia.

In each case an amorphous nanostructure, that forms the interior of the scales, has been identified as the source of the specimens' white appearance. Examining the scales of the three species by scanning electron microscope reveals the scales' internal structure. In each case an outer envelope of cuticle surrounds the disordered structure within. Both *Cyphochilus* and *L. stigma* exhibit a dense filamentary network within their scales (Fig. 10.5 (b) and (d)). Typically these filaments have diameters in the range 250–350 nm with a spacing of the order of 700 nm. Image analysis indicates a scale void filling fraction of approximately 50–70 %. The white elytral patches of *C. margaritifera* result from a thick covering of hair-like scales. The internal structure of these is unlike that previously described; rather than filamentary, this microstructure comprises disordered spheres aggregated together into clumps and filaments (Fig. 10.5(f)). Imaging of the structure indicates a sphere diameter of 300 nm and that the accumulated microstructure fills approximately 55 % of the scales internal void.

The amorphous nature of these microstructures results in broadband optical scatter, i.e. all wavelengths of light are reflected with approximately equal efficiency and as a result all three species exhibit a bright white colour appearance. In fact these species all exhibit remarkably efficient reflectance. A sheet of typical office paper has a thickness of 100 microns; this is approximately ten times the thickness of any of these beetle scales. Despite this, the paper only reflects between 5 % and 10 % more light when compared to the beetle scales. Such remarkable optical scatter from so little material indicates an exceptionally efficient and likely optimised scattering system. Optimisation of the scale microstructure design could manifest itself in one of three key parameters; the scale void filling fraction, the scattering centre size and the scattering centre spacing. Where optimisation of these key parameters is evident, strong optical scatter and bright white reflectance occur.

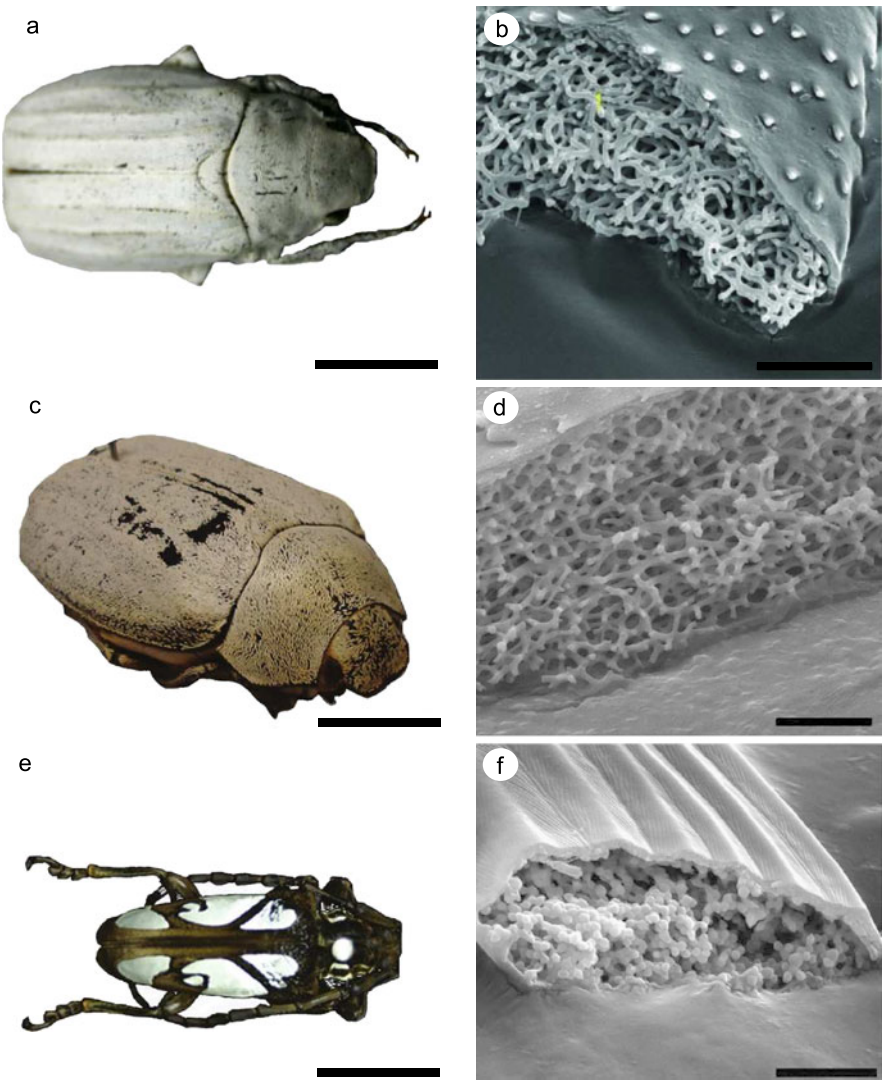

Fig. 10.5 (**a**) The scarab beetle *Cyphochilus* derives its exceptional whiteness from a covering of scales. (**b**) SEM of a single *Cyphochilus* scale revealing its highly disordered microstructure. (**c**) and (**d**) Another scarab beetle *Lepidiota stigma* exhibits both similar whiteness and a similar disordered scale microstructure. (**e**) The gloss white eltyral patches of the longhorn beetle *Calothyrza margaritifera* are also the result of a scale covering. (**f**) With the scales of *C. margaritifera* is a disordered structure unlike that of the scarab species previously described. *Scale bars*: (**a**), (**c**) and (**e**): 1 cm. (**b**), (**d**) and (**f**): 4 μm

The amount of material contained within the scale void appears to be the key parameter that influences the scattering efficiency of the scale. Finite element modelling has been used to simulate the scale structures of the three species and to

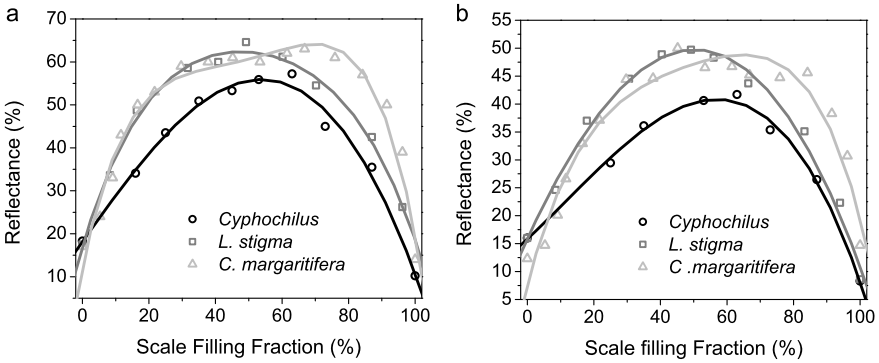

Fig. 10.6 Finite element modelling results which indicate that the scales of each of the three beetles are approximately optimised in terms of scale void filling fraction. In each case the peak in the curve approximately coincides with the scale void filling fraction of each species measured from TEM images. (**a**) TE polarised illumination, (**b**) TM polarised illumination. In each case the *solid line* represents a best fit to the modelled data points

probe the influence of scale void filling fraction on optical scatter. Computational limitations and the highly complex nature of the structures limited modelling to two dimensions. The models were generated by image manipulation of TEM images of transverse slices through the structure. Varying the size of the air pores within these original models varied the filling fraction [44].

Transmission and reflectance were simulated for both TE and TM incident light at normal incidence. The 2D model geometry is set out in the XY plane with the Z-plane defined as into the page. In this geometry, TE incident radiation is defined as the electric vector perpendicular to the XY plane. TM radiation is therefore defined as the electric vector parallel to the XY plane. Whilst reducing the dimensionality of the model was a computational requirement, it does not appear to change the conclusions that can be drawn from the modelled data. In reducing the dimensionality we have removed a component of disorder from the model. The remaining 2D model, however, remains fundamentally disordered. This method may result in a slight reduction in the intensity of the optical scatter modelled, but otherwise accurately models the optical scattering phenomena in question and does not modify the conclusions that can be drawn from the models. The modelled reflectance profiles obtained from the process described above are displayed in Fig. 10.6 for both incident TE radiation (Fig. 10.6(a)) and incident TM radiation (Fig. 10.6(b)).

While the absolute values of the modelled reflectance are not the same for both polarisations, the modelled reflectance vs. scale void filling fraction profiles are very similar. For each species there is a good agreement between the simulated filling fractions at which peak reflectance occurs and the actual measured filling fractions. For TE incident radiation, the modelled filling fraction of *Cyphochilus* scales which results in peak reflectance is 63 ± 6 %. This is very close to the 68 ± 7 % filling fraction of actual *Cyphochilus* scales, measured over a large number of TEM sections. This indicates that approximately 63 % is the optimum filling fraction for

the filamentary system within *Cyphochilus* scales. Analogous modelling was carried out for the scale microstructures of *L. stigma* and *C. margaritifera* (also plotted in Fig. 10.6 (a) and (b)). These results indicate that the optimum filling fraction is not independent of the other microstructure parameters; the optimum filling fraction appears to change when a different filament diameter is considered. *L. stigma* scales also appear to exhibit an optimal filling fraction, which at 48 ± 3 % is significantly different to the optimised filling fraction of *Cyphochilus* scales. *L. stigma* scales have filaments with a diameter of approximately 350 nm, compared to a diameter of 250 nm for *Cyphochilus* filaments. It appears that this difference in filament design is responsible for the difference in optimal filling fraction.

The different microstructure of *C. margaritifera* appears to result in a different reflectance vs. filling fraction profile. For both polarisations it is apparent that for this structure, a small variation in reflectance is observed for a wide range of scale filling fractions. This is noticeable for scale filling fractions in the range 35 to 75 %, where very little change in modelled reflectance is observed. This suggests that while a filling fraction in the range 35–75 % is essential for optimal light scatter, it is far less critical for the particle based scattering system of *C. margaritifera* than it is for the filamentary based systems of *Cyphochilus* and *L. stigma*.

Within the microstructures identified, the individual filaments and spheres can be considered as individual scattering units. The size and spacing of these units influences the optical scatter from the system as a whole. The effect of individual scattering element diameter on overall reflectance was investigated using a Mie theory model of a homogeneous sphere with a varying diameter. Three wavelengths representing key colours of the visible spectral range were used in the modelling process. For each sphere diameter, the radiation which was scattered into the reflection hemisphere was integrated and is depicted for each of the three wavelengths in Fig. 10.7(a).

The results of this modelling imply that for wavelengths covering the entire visible spectrum there is an optimum scattering centre diameter which leads to maximised optical scatter. The data suggest that for visible wavelengths, this optimum diameter is in the range 200–300 nm. SEM image analysis carried out previously has revealed that the filaments within the scales of *Cyphochilus* and the spheres within the scales of *C. margaritifera* fall within this size range, implying that their scattering structures are optimally sized to ensure maximal optical scatter from their scales. Interestingly, the filaments within the scales of *L. stigma* have a diameter which does not fall into the optimum range identified here, this is assumed to be the reason for *L. stigmas* apparent poor optical efficiency when compare to *Cyphochilus* and *C. margaritifera*.

The effect of scattering centre spacing on the optical properties of a sample was investigated using synthetic partical-based scattering systems. Blends of titanium dioxide (TiO_2) and solid latex spheres were coated onto base paper in different blend ratios. The fabricated system could be considered as a set of monosized spheres in which the blend ratio between TiO_2 and latex determined the average spacing between TiO_2 particles. Each fabricated system was immersed in matching fluid, blended to optically match the refractive index of the latex spheres, leaving the TiO_2

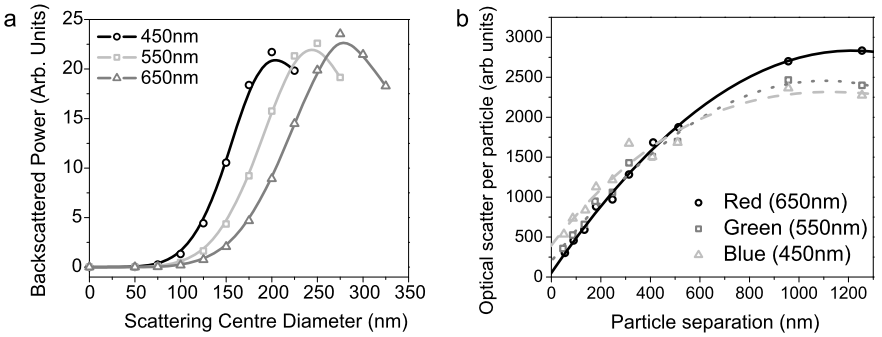

Fig. 10.7 (**a**) Mie theory back scattering results which indicate an optimum centre size for maximum scattering efficiency of visible wavelengths to be approximately 200–300 nm. The beetle scale microstructures have scattering elements (fibrils or particles) that fall within this size range, suggesting optimisation for maximal optical scatter. (**b**) Similar optimisation is apparent with the scattering centre spacing, in the beetle species this is typically 600–700 nm. Optical scatter from synthetic systems indicate this is within an approximately optimal range of 500–700 nm. In both cases, the *lines* represent best fits to the data points

particles in an optically homogeneous medium. Reflectance spectra were taken from each system and Kubelka–Munk theory [23] was used to calculate the light scatter contribution of the individual TiO_2 particles as a function of their spacing.

The optical scatter data collected during this experiment is presented in Fig. 10.7(b). The data reveal that the contribution to optical scatter from each individual scattering particle falls as the particles are moved closer together. The optimum surface-to-surface spacing appears to be approximately 1200 nm, but the most dramatic reduction in light scatter contribution occurs below a surface-to-surface separation of approximately 500 nm. This reduction in scattering efficiency is due to the phenomenon of optical crowding [42, 43]. As the particles are moved closer together the incident light is no longer scattered by the individual particles, instead it is effectively scattered from a larger single particle with subsequent lower scattering efficiency. The data show that the wavelength of incident light has very little effect on this phenomenon.

While avoiding optical crowding is vital for strong optical scatter from a particle-based system, a reciprocal problem must also be addressed. To ensure high optical scatter per scattering centre, the scatterers must be relatively sparsely distributed. In a finite sample, however, this leads to a low spatial density of scattering centre leading to low overall light scatter. Therefore any attempt to overcome the loss in scattering efficiency due to optical crowding must be balanced against the reciprocal loss in total scatter associated with fewer scattering centres per unit volume. The optimum compromise between the two effects appears to occur at an inter-particle spacing of approximately 500–600 nm. At this spacing the scattering particle spatial density is relatively high and dominates over the negative effects of optical crowding.

The filamentary structures identified within the scales of *Cyphochilus* and *L. stigma* differ from these systems as they are based on a connected system, unlike

the discrete particle systems fabricated here. However, the systems can be considered analogous because an inter-filament spacing which is too small will lead to a similar optical crowding problem. The filament spacing of *Cyphochilus* and *L. stigma* were measured at 580 ± 120 nm and 700 ± 180 nm respectively, where the error margin quoted is the standard deviation of many ($n = 50$) measurements. This indicates that the filaments are approximately optimally spaced to maximise optical scatter. Optical crowding is largely avoided, while scattering centre density is kept high.

In any amorphous medium designed for efficient broadband optical scatter, there is a fine balance between achieving the maximum scattering-centre density, while maintaining sufficient scattering-centre spacing. If the scattering centres are placed too close together, optical crowding will occur. Balanced against this is the need to maintain sufficient scattering centre number density. If the scattering centres are spaced too far apart, their number density will fall and this will also result in a loss of light scatter. There must clearly be a compromise between these two effects in order to create the most efficient scattering system. Experimental data and theoretical modelling indicate that the scattering microstructures within the scales of *Cyphochilus*, *L. stigma* and *C. margaritifera* have evolved into systems with structural variations that achieve an optimal compromise in this way. Further to this, Mie theory modelling and experimental scattering data indicate that scattering centres with a diameter of 200–300 nm and mutual distance of approximately 500 nm reach an optimal size and spacing. Our SEM and TEM analyses indicate that the microstructures within the scales of all three species are typically within these size and spacing ranges, further implying structural optimisation.

Further compromises in design may also hamper the optical function of beetle scale. Specifically here, for these white beetles, the ultra-thin microstructures in their scales must scatter light efficiently for bright whiteness but must concurrently be relatively light so as not to add unnecessary weight. Additionally, the material itself must be robust enough to limit abrasive damage during the beetle's lifetime.

The bright white colour of these beetles is understood to serve the same primary functions ascribed to most colouration strategies used by animals; namely to communicate with conspecifics or to avoid predation [45]. While bright whiteness may seem counter-intuitive as a cryptic colour in *Cyphochilus*, their natural habitat has been linked to areas rich in white fungi [41]. Their white appearance may therefore aid in predator avoidance. Colour appearance often has a multifunctional role and colours may evolve in response to two or more, often contradictory, selection pressures [46]. While acting as a cryptic colour, the bright whiteness may also aid conspecific recognition. Colour appearance is known to serve other non-visual functions such as thermoregulation [33]. Certainly, it has been shown that any form of dorsal colouration has consequences for thermoregulation in specific species of diurnal beetles [33]. Hadley et al. [46] found that white morphs of the beetle *Neocicindela perhispida* were able to forage for longer without overheating when transferred from their natural white sand habitat to a black sand terrain, compared to the native black morphs of the same species, which escaped the heat by burrowing into the sand.

10.3 Non-insect Examples

10.3.1 White Hairs on the Edelweiss Plant

Leotopodium nivale alpinium (edelweiss) is an herbaceous plant found in the European mountains at altitudes up to 3400 m. In this harsh environment the plant is subject to very dry and windy conditions. The whole plant, including stems, leaves, bracts and flowers are found to be abundantly covered in felt-like hair. This hair is thought to protect the plant through limiting water evaporation. Recent work suggests that the white hairs also play a secondary protection role; they limit the plants' exposure to the high flux of harmful UV radiation in the rarefied high-altitude atmosphere [47].

Investigation of the white covering reveals a 'criss-cross' of hairs, some millimetres in length and with a diameter of approximately 10 μm. SEM imaging of the hair reveals longitudinal filaments running the length of the hairs, spaced in such a manner that they form a diffraction grating-like structure on the surface. The filaments have a size of 180 nm, appropriate for manipulation of UV radiation [47].

Optical measurements of the hair both *in vivo* and when removed from the plant reveal exceptionally broadband reflectance, in line with their white colour. When reflection and transmission are compared similar trends are observed, namely very little UV reflection or transmission. Nearly 100 % of the UVA radiation (300–400 nm) is absorbed by the white hair covering [47].

In this case the term 'absorbed' is used to describe radiation which loses energy while transiting through the filament walls and also radiation which first turns into guided modes in a Fano-resonance process and then disappears with the lifetime of the guided mode. Theoretical models, which approximate the hair surface as a flat diffraction grating, indicate that the filaments allow the incident radiation to excite guided modes which allows the electromagnetic energy to propagate over a much larger distance. It is unclear what the actual absorption mechanism is, whether it takes place within the filament wall itself or whether the core of the hair contains an absorbing compound. One suggested compound is water which has excellent UV absorbing properties [47].

Photonic structures are not common in plants but this example highlights the potential gain from employing photonic strategies. The fleece covering of the plant protects the organism from not only both cold and drought, but harmful UV radiation as well. A photonic structure has evolved which uses diffraction effects to preferentially dissipate UV radiation by allowing the effective energy exchange from the incident wave to guided modes.

10.3.2 Disordered Multilayer Systems

Camouflage, as a means of survival, is highly developed in fish and provides another interesting example of a 'chaotic' reflector system. The most common fish colour

appearance is broadband silver; this provides camouflage against the silvery hue of the water surface when viewed from below. In fish, colour appearance is usually attributed to reflection from multilayer stacks (1D photonic crystals) [48]. Multilayering is typically associated with bright saturated (narrowband) colours, but with subtle alterations to the periodic system can bring out a broadband response. Three different perturbations to an ideal quarter-wave plate stack result in broadband reflectance; the use of multiple filters with different spacing, a chaotic multilayer with a random distribution of layer thicknesses and finally a 'chirped' multilayer with an increasing or decreasing layer thickness [31, 33]. The first method is common and is thought to explain the silver colour of many fish species. Of more interest to this chapter is the 'chaotic' system where a random distribution of later thicknesses results in an ultra-broadband response.

Two species of the family *Trichiurodae*, the 'hairtail' and the 'ribbonfish', exhibit such a chaotic reflector. Identified by McKenzie et al. [49], these species were found to reflect approximately 65 % of light from 400 nm right up to well over 1000 nm, an incredibly broad range over which to exhibit such a constant reflectance. Computational modelling using the multiple filter method (with 3 filters with responses centres on 500, 800 and 1100 nm) was found to recreate the observed colour, but not the actual reflectance spectrum. Multilayer systems which consist of alternating layers of high and low refractive index layers and randomly varying optical thickness have been studied and give rise to a phenomenon known as *optical localisation*. The reflected waves generated at the interfaces interfere in such a way that the electromagnetic wave is confined to a region known as the *localisation length*. If the thickness of the system is greater than the localisation length then the propagation of light through the system is prohibited. In the case of non-absorbing material, the incident radiation can then only be reflected [49]. Computational models using high refractive index layers of 1.83 (Guanine) with thicknesses in the range 55–165 nm and low index layers of 1.33 (Cytoplasm) with thicknesses in the range 75–225 nm, and a total thickness of 200 layers (26 μm) were generated. Ten multilayer stacks were generated and the results averaged, giving a good qualitative match to optical measurements. TEM imaging of cross-sections through the skin of the ribbonfish confirms the chaotic reflector system [49].

The random multilayer stack is distinctly different from a quarter wave stack in that the quarter-wave stack is notable for its exceptional efficiency with very few layers but only over a very narrow band. This is undesirable in a system which is trying to achieve a broadband response with a limited material choice. In fish there is little constraint on the thickness of the system so the efficiency of a quarter wave stack brings no advantage, a disordered system is a much more likely result given the beneficial broadband response it brings [49].

10.4 Conclusions

In response to a range evolutionary selection pressures many species have developed complex microstructure based colour appearance mechanisms. In the majority

of systems, alternating layers of high and low refractive index result in a surface with a high reflectivity and a bright saturated colouration. Higher degrees of order (2D and 3D photonic crystals) typically results in a similar optical narrow-band coloured reflectance. In order to achieve a broadband reflectance, usually resulting in a white colour appearance, an amorphous (disordered) structure is typically required. Such amorphous structures are not as common in nature as their more ordered counterparts, but some such systems have been identified. The Pierid family of butterflies ('whites and sulphurs') contains many examples of such colour appearance. In this case the disorder is in the form of a dense array of nanoscopic beads which significantly enhance optical scatter of all visible wavelengths, resulting in a broadband, and thus white, response. Amorphous structures have also been identified in several species of beetle. In these cases ultra-thin scales exhibit exceptional whiteness and brightness using a minimal thickness of scattering structure. Such efficiency suggests an optimised scattering structure. Investigation of the structure has confirmed the high degree of optimisation.

With such efficient systems identified it is of little surprise to learn of possible bio-mimetic applications of such microstructure. The filamentary structure of *Cyphochilus* in particular has been of interest. With only 5 μm of material this structure out performs many synthetic systems containing far more material, mimicking its structure and its optimisation could potentially lead to optical advances applicable to many technologies. With so many species from which to choose, including those of plants, fish and insects, there is still a wealth of natural resources that will inspire emerging and future optical technology.

References

1. P. Vukusic, *Optical Interference Coatings*, Natural Coatings (Springer, Berlin, 2003)
2. R. Hooke, Micrographia: or some physiological descriptions of minute bodies made by magnifying glasses, in *Project Gutenberg* (1665)
3. I. Newton, Opticks: Or a Treatise of the Reflexions, Refractions, Inflexions and Colours (Royal Society, London, 1704)
4. L. Rayleigh, On the reflection of light from a regularly stratified medium. Proc. R. Soc. Lond., a Contain. Pap. Math. Phys. Character **93**(655), 565–577 (1917)
5. L. Rayleigh, On the optical character of some brilliant animal colours. Philos. Mag. **37**(217) (1919). doi:10.1080/14786440108635867
6. P. Vukusic, J. Sambles, C. Lawrence, R. Wootton, Quantified interference and diffraction in single Morpho butterfly scales. Proc. R. Soc. Lond. B, Biol. Sci. **266**(1427), 1403 (1999)
7. T. Trzeciak, P. Vukusic, Photonic crystal fiber in the polychaete worm *pherusa sp.* Phys. Rev. E **80**(6), 061908 (2009)
8. C. Pouya, D. Stavenga, P. Vukusic, Discovery of ordered and quasi-ordered photonic crystal structures in the scales of the beetle *eupholus magnificus*. Opt. Express **19**(12), 11355–11364 (2011)
9. C. Mason, Structural colors in insects. I. J. Phys. Chem. **30**, 383–395 (1926)
10. H. Ghiradella, Structure of *iridescent lepidopteran* scales: variations on several themes. Ann. Entomol. Soc. Am. **77**(6), 637–645 (1984)
11. H. Ghiradella, Structure of butterfly scales: patterning in an insect *cuticle*. Microsc. Res. Tech. **27**(5), 429–438 (1994)

12. H. Ghiradella, D. Aneshansley, T. Eisner, R. Silberglied, H. Hinton, Ultraviolet reflection of a male butterfly: interference color caused by thin-layer elaboration of wing scales. Science **178**(4066), 1214 (1972)
13. H. Ghiradella, Hairs, bristles, and scales. Microsc. Anat. Invertebr. **11**, 257–287 (1998)
14. M. Giraldo, D. Stavenga, Sexual dichroism and pigment localization in the wing scales of *Pieris rapae* butterflies. Proc. R. Soc. Lond. B, Biol. Sci. **274**(1606), 97 (2007)
15. F. Lutz, 'Invisible' colors of flowers and butterflies. Nat. Hist. **33**, 565–576 (1933)
16. K. Makino, K. Satoh, M. Koike, N. Ueno, *Sex in Pieris Rapae L. and the Pteridin Content of Their Wings* (1952)
17. B. Wijnen, H. Leertouwer, D. Stavenga, Colors and pterin pigmentation of pierid butterfly wings. J. Insect Physiol. **53**(12), 1206–1217 (2007)
18. J. Kolyer, A. Reimschuessel, Scanning electron microscopy on wing scales of *Colias eurytheme*. J. Res. Lepid. **8**, 1–15 (1970)
19. N. Morehouse, P. Vukusic, R. Rutowski, Pterin pigment granules are responsible for both broadband light scattering and wavelength selective absorption in the wing scales of pierid butterflies. Proc. R. Soc. Lond. B, Biol. Sci. **274**(1608), 359 (2007)
20. N. Yagi, Note of electron microscope research on pterin pigmentation in *pierid* butterflies. Annot. Zool. Jpn. **27**, 113–114 (1954)
21. R. Rutowski, J. Macedonia, N. Morehouse, L. Taylor-Taft, Pterin pigments amplify iridescent ultraviolet signal in males of the orange sulphur butterfly, *Colias eurytheme*. Proc. R. Soc. B **272**(1578), 2329 (2005)
22. D. Stavenga, S. Stowe, K. Siebke, J. Zeil, K. Arikawa, Butterfly wing colours: scale beads make white pierid wings brighter. Proc. R. Soc. Lond. B, Biol. Sci. **271**(1548), 1577 (2004)
23. P. Kubelka, F. Munk, Ein beitrag zur optik der farbanstriche. Z. Tech. Phys. **12**, 593–601 (1931)
24. S. Luke, P. Vukusic, B. Hallam, Measuring and modelling optical scattering and the colour quality of white pierid butterfly scales. Opt. Express **17**(17), 14729–14743 (2009)
25. Y. Obara, Studies on the mating behavior of the white cabbage butterfly, *Pieris rapae crucivora Boisduval*. J. Comp. Physiol. A: Neuroethol. Sens. Neural Behav. Physiol. **69**(1), 99–116 (1970)
26. R. Rutowski, The use of visual cues in sexual and species discrimination by males of the small sulphur butterfly *Eurema lisa* (lepidoptera, pieridae). J. Comp. Physiol. A: Neuroethol. Sens. Neural Behav. Physiol. **115**(1), 61–74 (1977)
27. Y. Obara, M. Majerus, Initial mate recognition in the British cabbage butterfly, *Pieris rapae rapae*. Zool. Sci. **17**(6), 725–730 (2000)
28. D. Kemp, P. Vukusic, R. Rutowski, Stress-mediated covariance between nano-structural architecture and ultraviolet butterfly coloration. Ecology **20**, 282–289 (2006)
29. S. Kinoshita, S. Yoshioka, K. Kawagoe, Mechanisms of structural colour in the *Morpho* butterfly: cooperation of regularity and irregularity in an iridescent scale. Proc. R. Soc. Lond. B, Biol. Sci. **269**(1499), 1417 (2002)
30. S. Yoshioka, S. Kinoshita, Structural or pigmentary? Origin of the distinctive white stripe on the blue wing of a *Morpho* butterfly. Proc. R. Soc. Lond. B, Biol. Sci. **273**(1583), 129 (2006)
31. A. Parker, D. Mckenzie, M. Large, Multilayer reflectors in animals using green and gold beetles as contrasting examples. J. Exp. Biol. **201**(9), 1307 (1998)
32. J. Vigneron, J. Colomer, N. Vigneron, V. Lousse, Natural layer-by-layer photonic structure in the squamae of *Hoplia coerulea* (*Coleoptera*). Phys. Rev. E **72**(6), 61904 (2005)
33. A. Seago, P. Brady, J. Vigneron, T. Schultz, Gold bugs and beyond: a review of iridescence and structural colour mechanisms in beetles (Coleoptera). J. R. Soc. Interface **6**(suppl 2) (2009). doi:10.1098/rsif.2008.0354.focus
34. T. Anderson, A. Richards Jr, An electron microscope study of some structural colors of insects. J. Appl. Phys. **13**, 748 (1942)
35. C. Mason, Structural colors in insects. II. J. Phys. Chem. **31**(3), 321–354 (1927)
36. A. Parker, V. Welch, D. Driver, N. Martini, Structural colour: opal analogue discovered in a weevil. Nature **426**(6968), 786–787 (2003)

37. V. Welch, J. Vigneron, Beyond butterflies—the diversity of biological photonic crystals. Opt. Quantum Electron. **39**(4), 295–303 (2007)
38. P. Vukusic, R. Kelly, I. Hooper, A biological sub-micron thickness optical broadband reflector characterized using both light and microwaves. J. R. Soc. Interface **6**(Suppl 2), S193 (2009)
39. M. Srinivasarao, Nano-optics in the biological world: beetles, butterflies, birds, and moths. Chem. Rev. **99**(7), 1935–1962 (1999)
40. T. Hariyama, M. Hironaka, H. Horiguchi, D.G. Stavenga, The leaf beetle, the jewel beetle and the damselfly; insects with a multilayers show case, in *Structural Colors in Biological Systems: Principles and Applications* (Osaka University Press, Osaka, 2005)
41. P. Vukusic, B. Hallam, J. Noyes, Brilliant whiteness in ultrathin beetle scales. Science **315**(5810), 348 (2007)
42. F. Steig, Ending the 'crowding/spacing theory' debate. J. Coat. Technol. **59**, 96–97 (1987)
43. J. Braun, Crowding and spacing of titanium dioxide pigments. J. Coat. Technol. **60**(758), 67–71 (1988)
44. S. Luke, B. Hallam, P. Vukusic, Structural optimization for broadband scattering in several ultra-thin white beetle scales. Appl. Opt. **49**(22), 4246–4254 (2010)
45. S. Doucet, M. Meadows, Iridescence: a functional perspective. J. R. Soc. Interface **6**(Suppl 2), S115 (2009)
46. N. Hadley, A. Savill, T. Schultz, Coloration and its thermal consequences in the New Zealand tiger beetle *Neocicindela perhispida*. J. Therm. Biol. **17**(1), 55–61 (1992)
47. J. Vigneron, M. Rassart, Z. Vértesy, K. Kertész, M. Sarrazin, L. Biró, D. Ertz, V. Lousse, Optical structure and function of the white filamentary hair covering the edelweiss bracts. Phys. Rev. E **71**(1), 011906 (2005)
48. E. Denton, M. Land, Mechanism of reflexion in silvery layers of fish and cephalopods. Proc. R. Soc. Lond. B, Biol. Sci. **178**(1050), 43–61 (1971)
49. D. McKenzie, Y. Yin, W. McFall, Silvery fish skin as an example of a chaotic reflector. Proc. R. Soc. Lond. Ser. A, Math. Phys. Sci. **451**(1943), 579 (1995)